J Electr Eng Technol.2015; 10(3): 1048-1057
http://dx.doi.org/10.5370/JEET.2015.10.3.1048

ISSN(Print) 1975-0102
ISSN(Online) 2093-7423

Parallel Sensorless Speed Control using Flux-axis Current for Dual SPMSMs Fed by a Single Inverter

Chang-Bum Kim*, Chul Yun, Byung-Keun Yoon**, Nae-Soo Cho*** and Woo-Hyen Kwon†**

Abstract – This paper proposes a sensorless speed control algorithm for parallel-connected dual Surface-mounted Permanent Magnet Synchronous Motors (SPMSMs) fed by a single inverter. For stable parallel operation of synchronous motors with a single inverter, each motor has to be constantly kept in the synchronization state regardless of load torque. If the master motor with the larger load is controlled, the synchronous state will be maintained. Therefore, detection of the master motor is essential. Conventionally, the master motor is determined by comparing the rotor position error from the relation between the back-EMF for torque angle and the flux position; consequently, the position sensor is deemed essential for finding the rotor position. The parallel sensorless speed control method proposed in this paper uses no position sensor, instead it compares the flux-axis current from the connection between the back-EMF for torque angle and current in unbalanced load conditions. The results of simulation and experiment conducted verify the efficacy of the proposed method.

Keywords: Dual SPMSMs, SIMM, Select control, Sensorless speed control

1. Introduction

The importance of efficient use of energy in all industrial sectors is becoming more apparent with each passing day. To achieve this, productive and quality improvement is required in industries, which necessitates the use of high efficiency electric motors and systems, along with reduction in production costs.

In general, industrial products such as subways, air-conditioning systems, and home appliances use Surface-mounted Permanent Magnet Synchronous Motors (SPMSMs), which are highly efficient and possess wide ranging variable speeds, for their motor drive systems. In fields that do not require relatively precise torque control, such as air-conditioning systems in particular, speed, which is not affected by the load fluctuation, is the main control objective.

Conventionally, induction motors are used in parallel motor drive systems. Induction motors are able to operate in parallel when the rotational speed is different from the input frequency by slip control because they are asynchronous [1-3]. In contrast, SPMSMs are synchronous and so their rotors have to be synchronized with the input frequency.

† Corresponding Author: School of Electronics Engineering, Kyung-pook National University, Korea. (whkwon@ee.knu.ac.kr)
* AE Control Lab, LG Electronics/School of Electronics Engineering, Kyung-pook National University, Korea. (Patrick.kim@lge.com)
** School of Electronics Engineering, Kyung-pook National University, Korea. (yunchul@knu.ac.kr , gksjwl@nate.com)
*** Dept. of Electronics Information, Keimyung College University, Korea. (nscho0104@lycos.co.kr)
Received: September 11, 2014; Accepted: January 22, 2015

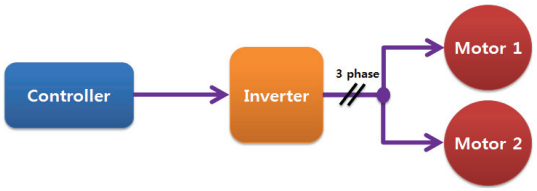

Fig. 1. Structure of a Single Inverter Multi-Motor (SIMM) system

Accordingly, in order to drive multiple SPMSMs via multiple inverters rotor position detection sensors are required. This increases the overall product size, volume, and production costs. To solve this problem, several methods for driving multiple motors with a single inverter, as shown in Fig. 1, have been proposed [4-9].

Conventional proposals can be classified into two categories: In the first category, SPMSMs arranged in parallel are connected to a single inverter that controls the average energy between them. This method has advantage of simple implementation because it uses the amount of energy change in accordance with the load as its control input. Consequently, it is able to operate in parallel within a suitable range of unbalanced load conditions. However, heat and noise measures for the switching device pose difficulties because load variation between two motors causes changes in the switch state transition point such that switching frequency varies when the inverter is controlled with a hysteresis comparator. Moreover, there may be a limit cycle interval in which the switching frequency increases rapidly in a low-speed driving area, in which the back-EMF is small, by selecting effective voltage continuously. This has the disadvantage of increased computation because

of the need to compose each controller to average the energy of the motors [4-7].

In the second category, both motors are connected to single inverter in parallel; however, the control signal from the inverter is designed only for the heavy load motor. In this scenario, the heavy load motor is defined as the master and the remaining motor as slave. The master motor is determined by comparing the rotor positon error with the hysteresis comparator from the relation between the back-EMF for torque angle and magnetic flux position. The motors perform in parallel with high reliability, since only the motor with the larger load is controlled, so both motors can maintain synchronization state always. Another advantage of this control method is simple system configuration with reduced computation by one controller [8, 9]. However, position sensors are essential for selecting the master motor from the detected rotor position of each motor. The position sensors raise structural problems such as vulnerability to vibration and shock and so it negates the benefits of having a single inverter with a parallel motor system. To overcome the disadvantageous of using speed sensor, this paper uses sensorless algorithm. Among the various sensorless algorithm, back-EMF based sensorless algorithm is reasonably chosen, since it is widely used in the industrial field [10-14].

In the case of a sensorless system, the rotor position has to be obtained from the sensorless algorithm in order to choose the controlling motor, since the sensorless algorithm calculates the rotor position by integrating the speed, the dynamic properties of the system are degraded because of time-delay problem in rapid load variation conditions. Since the purpose of comparison of the rotor is position error, a hysteresis comparator is used. Furthermore the hysteresis controller is used to compare the rotor position error; and the on/off switching time of the hysteresis width varies according to load oscillation and the drive system. This causes the system to enter rapid transient and unstable states. Therefore, the hysteresis width has to be adjusted by experienced experts to ensure stable operation of the system [8, 9].

Considering the advantages and disadvantages of the methods outlined above, the latter is better for application to industrial sites as a result of the simplicity of its control system and the ease of hardware configuration. However, as mentioned previously, this method has problems related to use of a hysteresis controller and speed sensor for determination of the load fluctuation between the motors. To overcome these drawbacks, this paper proposes a parallel drive sensorless speed control technology fed by a single inverter that compares the flux-axis current from the relation between the back-EMF for torque angle and current to ensure stable operation in unbalanced conditions. Because the master is chosen according to the flux-axis current, which is actually measured, it has a faster dynamic characteristic and operates more stably during rapid load variations than the rotor position method.

2. System Analysis

2.1 Analytical model of SPMSM

The d-q axis inductance of SPMSM is the same regardless of rotor position by the uniform air-gap because of its cylindrical structure, in which a permanent magnet is attached to the surface of the rotor. The $d^r - q^r$ axis voltage equation for rotation at the real angular velocity is shown as Eq. (1):

$$\begin{aligned} v_{ds}^r &= R_s i_{ds}^r + \frac{d\lambda_{ds}^r}{dt} - \omega_r \lambda_{qs}^r \\ v_{qs}^r &= R_s i_{qs}^r + \frac{d\lambda_{qs}^r}{dt} + \omega_r \lambda_{ds}^r \\ \lambda_{ds}^r &= L_d i_{ds}^r + \phi_m \\ \lambda_{qs}^r &= L_q i_{qs}^r \end{aligned} \tag{1}$$

where, R_s is the stator resistance, $\lambda_{ds}^r, \lambda_{qs}^r$ is the $d^r - q^r$ axis linkage flux, and ϕ_m is the permanent magnet flux. Eq. (2) shows the torque equation divided by the rotor angular velocity of the mechanical output power:

$$T_e = \frac{P}{2}\frac{3}{2}\varphi_m i_{qs}^r \tag{2}$$

where, P indicates motor poles. The mechanical equation is derived by the torque equation (Eq. (2)), and is given as Eq. (3):

$$T_e - T_L = J_m \frac{d\omega_m}{dt} + B_m \omega_m \tag{3}$$

where, T_L is load torque, J_m is inertia, B_m is friction, and ω_m is mechanical angular velocity.

2.2 Dynamic stability analysis by the torque angle

The principle of power occurrence can be physically determined from the flux relationship by drawing a vector diagram such as that shown in Fig. 2.

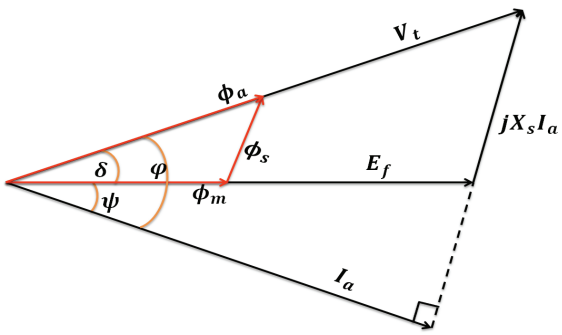

Fig. 2. SPMSM vector diagram

In Fig. 2, V_t is the armature voltage, I_a is the armature current, E_f is the excitation voltage, X_s is the synchronous reactance, ϕ_a is the air-gap flux, ϕ_m is the permanent magnet flux, ϕ_s is the armature reaction flux, φ is the power factor angle between V_t and I_a, Ψ is the inner power angle between I_a and E_f, and δ is the torque or power angle between V_t and E_f. The input power can be derived as Eq. (4) from the vector diagram in Fig. 2:

$$P = 3V_t I_a \cos\phi \tag{4}$$

The armature voltage can be derived from the vector diagram in Fig. 2. The torque-axis voltage is defined by Eq. (5), while the flux-axis voltage is defined by Eq. (6):

$$V_t \sin\delta = I_a X_s \cos(\phi - \delta) \tag{5}$$

$$V_t \cos\delta = E_f + I_a X_s \sin(\phi - \delta) \tag{6}$$

The armature current can be found from Eq. (7), which is derived from Eqs. (5) and (6):

$$I_a \cos\phi = \frac{E_f \sin\delta}{X_s} \tag{7}$$

Eq. (8) shows the mechanical output torque of the output power, found by substituting Eq. (7) into Eq. (4).

$$T = \frac{P}{\omega_m} = 3\frac{V_t E_f}{\omega_m X_s}\sin\delta = T_{\max}\sin\delta \tag{8}$$

Eq. (8) expresses the voltage and excitation voltage. Compared with the vector diagram in Fig. 2, the excitation voltage vector direction is the same as that of the permanent magnetic flux and the vector direction of the voltage is identical to the air-gap flux direction. Therefore, the maximum torque can be controlled by the excitation voltage when the voltage is kept constant. Fig. 3 illustrates Eq. (8) according to torque angle.

Output torque is determined by δ in the constant torque region, in which the voltage and excitation voltage area is fixed, as shown in Fig. 3. The maximum torque occurs at $\delta = 90^\circ$. If the torque angle is $\delta > 90^\circ$, the torque will lose the acceleration and the motor will be divergent [15].

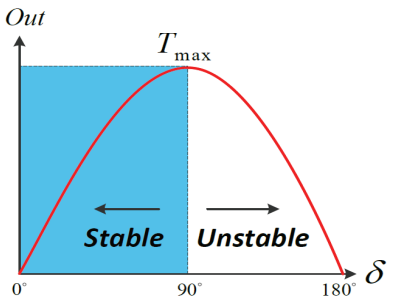

Fig. 3. Torque property according to δ

2.3 Load torque recognition method by flux-axis current

A vector diagram of a typical parallel-connected SPMSM at disagreement load state is depicted in Fig. 4 [5, 6]; the master motor is selected by relation between excitation voltage and flux position. In Fig. 4, M1 is the master motor and M2 is the slave motor. Because the load torque of M2 is greater than that of M1, $\delta_1 < \delta_2$ in Fig. 4(a). Conversely, in Fig. 4(b), because the load torque of M2 is smaller than that of M1, $\delta_1 > \delta_2$.

The master motor is determined based on the rotor position information of each motor. Thus, the rotor position detection sensor is an important component and the dynamic performance falls during load variation owing to time-delay in the sensorless system. For the purpose of reliable rotor location comparison, a hysteresis controller is used; however, it has the weakness that hysteresis width should be adjusted according to the drive system.

In contrast, the direction of the excitation voltage is the same as the permanent magnetic flux and the voltage vector path is equal to the air-gap flux route, as mentioned before.

Thus, from Eqs. (5) and (6), the torque-axis current and flux-axis current can be expressed as Eq. (9):

$$\begin{aligned} I_d &= I_a \sin(\phi - \delta) \\ I_q &= I_a \cos(\phi - \delta) \end{aligned} \tag{9}$$

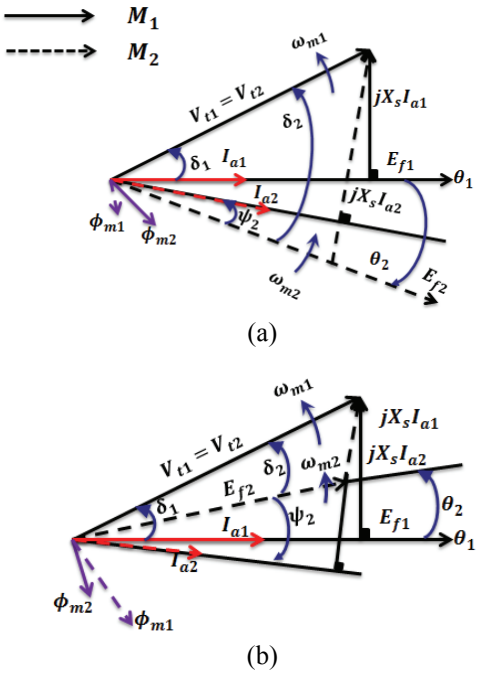

Fig. 4. Parallel connected SPMSM vector diagram: (a) Case 1: $T_{L1} < T_{L2}$, (b) Case 2: $T_{L1} > T_{L2}$

where, I_d is the flux-axis current and I_q is the torque-axis current. When the torque angle increases, the flux-axis current rises in the negative direction and the torque-axis current decreases, as shown in Eq. (9). It collapses the dynamic stability limit load torque. Therefore, in this paper, the load change is recognized by comparing the flux-axis current between the two motors.

$$\Delta i_d^r = i_{d\_m1}^r - i_{d\_m2}^r$$
$$\mathrm{sgn}\left[\Delta i_d^r\right] = \begin{Bmatrix} 1\left(\Delta i_d^r > 0\right) \\ 2\left(\Delta i_d^r < 0\right) \end{Bmatrix} \quad (10)$$

First, the error between the flux-axis current measured from the two motors is calculated using Eq. (10). The output of the sign function is one when the error is positive, otherwise the output is two. Thus, it is possible to select the feedback value control of the controller based on the sign function output. As a result, the controller controls the heavy load motor along with the sign function result, as shown in Fig. 5. On the other hands, if the load of master motor is bigger than slave one, the output of sign function is positive but slave one is bigger than the master motor then sign function output is negative by Eq. (10). As a result of that motor which has bigger load can be controlled by sign function output. Since the control motor is selected using flux-axis current, it can be applied to the sensorless system, and faster dynamic property can be obtained in load alteration because actual measured current is being used.

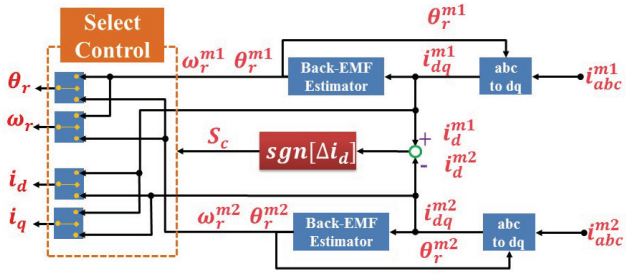

Fig. 5. Sensorless select control block diagram

3. Experimental evaluation

3.1 Simulation conditions

To verify the efficacy of the proposed method, parallel sensorless speed control system fed by a single inverter using SPMSMs flux-axis current, we simulated the algorithm. The sensorless speed control algorithm simulated estimates the rotor position and speed by back-EMF estimator using motor current [10, 11]. The simulation considered both steady-state and dynamic state characteristics.

First of all, torque angle and flux-axis current were

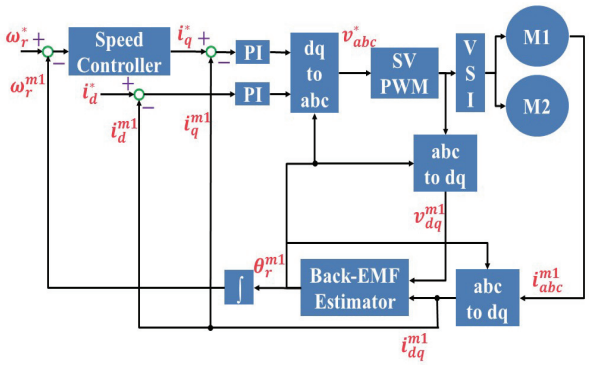

Fig. 6. SIMM structure without select control

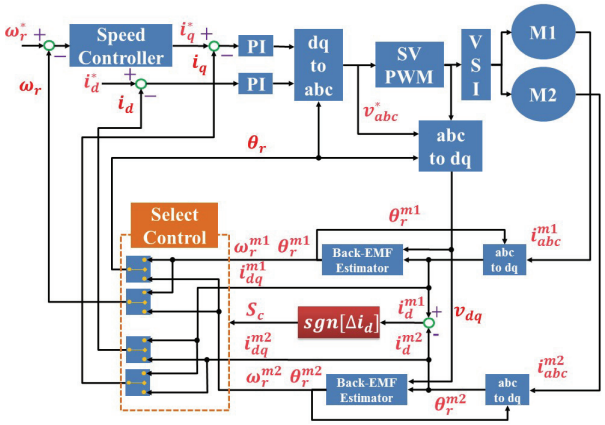

Fig. 7. Block diagram of the proposed system

observed so as to check the dynamic property of the parallel drive without select control, as shown in Fig. 6, by inserting load to M2.

Next, as indicated in Fig. 7, the dynamic characteristics of the proposed system, which has select control for parallel drive, were confirmed in like manner. The simulation was conducted using MATLAB/SIMULINK and the commonly used PI controller composed for current control. Voltage was modulated by a space vector PWM inverter, and rotor position, and speed information obtained from the back-EMF estimator. As shown in Fig. 5 and Eq. (10), select control by flux-axis current is realized.

Table 1 shows the SPMSM parameters.

Table 1. Nominal parameters for 26 W SPMSM

Base Speed	4000 rpm
R_s	0.6 Ω
L_s	0.17 mH
T_L	0.062 N.m
ϕ_m	0.0035 Wb
poles	8

Fig. 8 shows the block diagram for sensorless algorithm. Reference voltage is calculated with master motor rotating position for coordinate conversion since this paper controls only the master motor. However reference frame

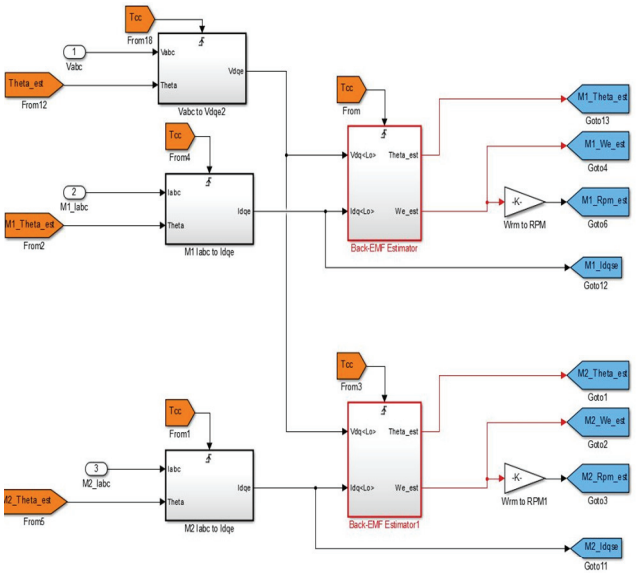

Fig. 8. Block diagram for sensorless algorithm

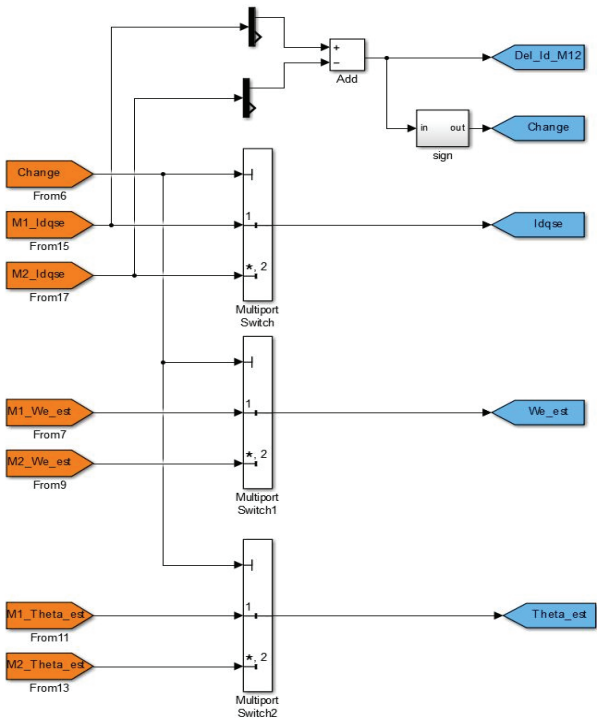

Fig. 9. Selection control block diagram

transformation for current uses the rotor positon of each motor.

Fig. 9 indicates the way to choose the master motor from d-axis current.

3.2 Simulation results

In order to approve the torque angle response of the slave motor for load change, in each simulation, a 5% increment of the rated torque was applied to only M2 at 0.6 s intervals, as illustrated in Fig. 6, during motor operation

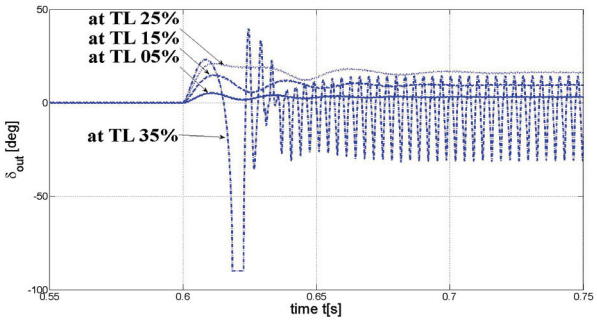

Fig. 10. Torque changes according to load torque

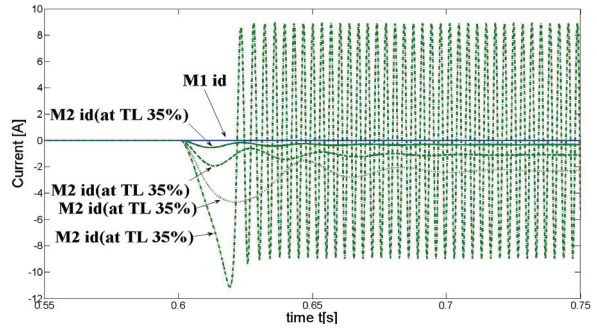

(a)

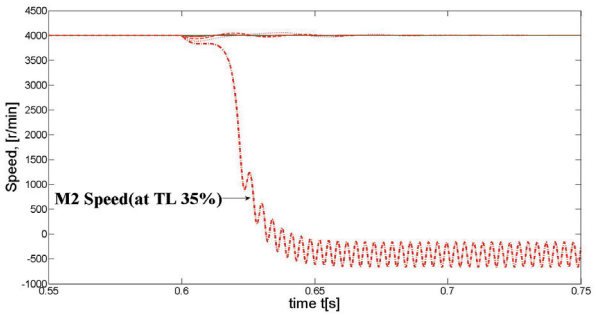

(b)

Fig. 11. Flux-axis current and speed by load change: (a) Flux-axis current response; (b) Speed response

at a rated speed of 4000 rpm in no-load condition. Fig. 10 displays the changes in output torque angle. M2 steps-out at 35% of rated torque. M2 should be deviated when a load torque is suddenly inserted even if it is lower than the rated torque.

In such a structure as Fig. 6, the dynamic stability limit of M2 is 25-30% of the rated load torque when the inverter output is no-load energy about M1. As shown in Fig. 11(a), back-EMF occurs in sync with the flux-axis in the transient state by load variation. The increment of the flux-axis current is negative until the motor steps-out according to load torque and the current vibrates with divergence.

Consequently, when a heavier load torque is applied to the slave motor than the motor being controlled, the slave motor cannot retain the synchronization state because the slave motor occurrence torque is lower than the required load torque owing to the reduced excitation voltage and

increased flux-axis current in the negative direction.

Motors simultaneously drive with rated speed command at 4000 rpm between 0-0.3 s in no-load condition. In the structure of the proposed method, illustrated in Fig. 12, the rated load torque is applied to only M2 at 0.6 s to verify the speed response in asynchronous load conditions for the motors to accelerate up to a rated speed of 4000 rpm between 0-0.3 s.

Fig. 12(b) shows the enlargement region A (around 0.6 s) of Fig. 12(a), while Fig. 12(c) illustrates the select signal by load change. At the transient state by load fluctuation, M1 speed vibrates around M2 speed and both motors become stable at the specified speed in 0.7 s, as shown in Fig. 12(b). A stable select signal occurs by comparing the flux-axis current about the unbalanced load from Fig. 12(c).

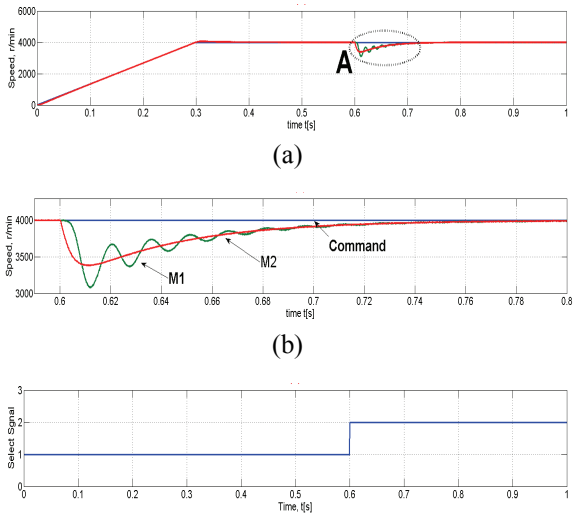

Fig. 12. Speed response in unbalanced load: (a) Speed response; (b) Zoom in region A; (c) Select signal

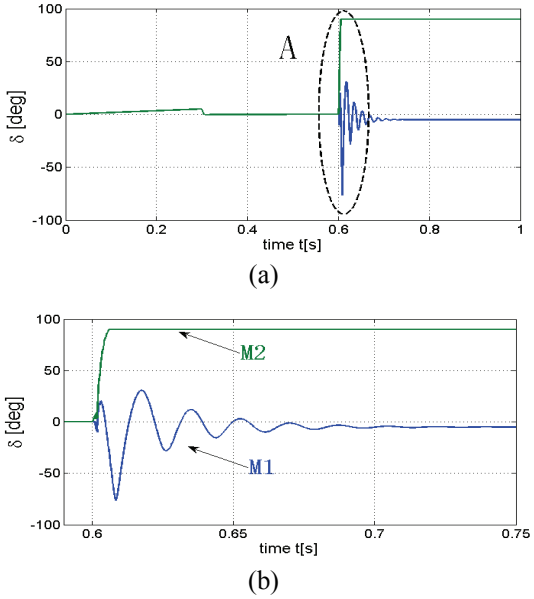

Fig. 13. Torque response in asynchronous load: Torque response; (b) Zoom in region A

Fig. 13 shows the torque angle of both motors about the disagreement load variation. Fig. 13(b) is a zoom of region A (around 0.6 s) of Fig. 13(a). Fig. 13(b) shows that M2 load torque is greater than that of M1 owing to M2 torque angle being 90° and M1 torque angle becoming -5° after shaking; thus, stable operation is possible for both motors.

3.3 Experimental conditions

For the purpose of examining the proposed method, an experimental system was constructed with two 26 W SPMSMs with the same specification as outlined in Table 1, inverter board, control board, and DAC for data analysis, as shown in Fig. 14.

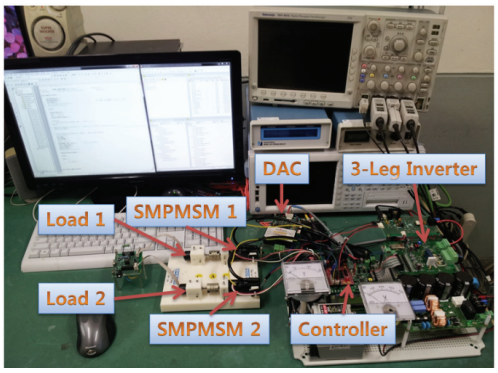

Fig. 14. Experiment construction

The proposed method and sensorless speed control software used in the experiment was designed in the same way with the simulation. The experiment was classified into three sections:

First, to confirm the speed response in no-load and unbalanced load conditions between the motors, step load torque was inserted by checking the speed response and select signal.

Second, to examine the speed response to rapidly disagreeing load change, high frequency load was set to only M1 and the speed response and select signal of both motors checked.

Third, the speed response and select signal were checked for different load changes in light load conditions during M1 control.

3.4 Experimental results

To verify the speed response for step load, the two motors operated at 2000 rpm in no-load condition. Sixty percent of the rated torque was set at 8 s for M1 and removed after 2 s. After 4 s, 60% of the rated torque was inserted to both motors and again removed in 2 s. Fig. 15(b) shows the expanded region A of Fig. 15(a), while Fig.

15(c) is the expanded region B of Fig. 15(a).

Fig. 15(b) illustrates the speed response according to the disagreement load of both motors, while Fig. 15(c) indicates the speed response for the synchronous load of both motors. Fig. 15(b) shows that the initial state of the select control is two until the rated speed controlling M2 is reached. When the load torque is inserted to M1 around 8 s the select signal output changes to one for M1 control. The settling time of the speed is 126 ms and the load response rate is 11.8% of steady-state speed.

Fig. 15(c) shows that M2 is under control when the load torque is removed by changing the select signal to two. The same load is applied to M1 and M2 simultaneously at 14 s, then M1 is controlled with one select signal.

The settling time is 126 ms and load response rate is 9.4% of steady-state speed. From the results of the experiment, it is clear that the speed can be controlled stably in balanced and unbalanced conditions during harmonious driving of two motors at the same speed. Next, to verify the high frequency load response, the motors were driven with a 2000 rpm command in no-load conditions. The magnitude was 25% of the rated torque and the frequency was 62.8 rad/s, with load torque set to M1 at 9 s and removed after 6 s.

Fig. 16(b) shows the enlarged region A of Fig. 16(a). Fig. 16(b) indicates the response for unbalanced high frequency load variation. The select signal outputs two initially to control M2. When the high frequency load is inserted to M1 at 9 s, the select signal wave along with load frequency and the controller alternately control M1 and M2.

The ripple rate of the stead-state speed appears at 3.75% of the specified speed. The experimental results show that stable operation is possible in rapid vibration asynchronous load conditions.

Finally, we checked the speed response by disagreement load variation for the two motors driven with light load while controlling M1 at 2000 rpm speed. Sixty percent of

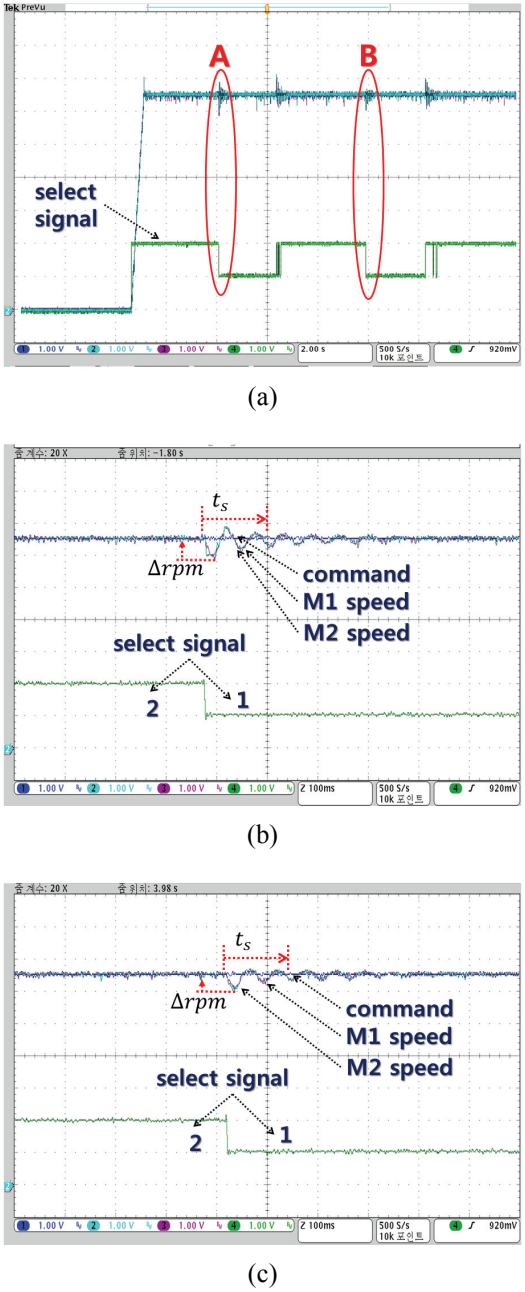

Fig. 15. Speed response by system load: (a) Speed response; (b) Zoom in region A; (c) Zoom in region B

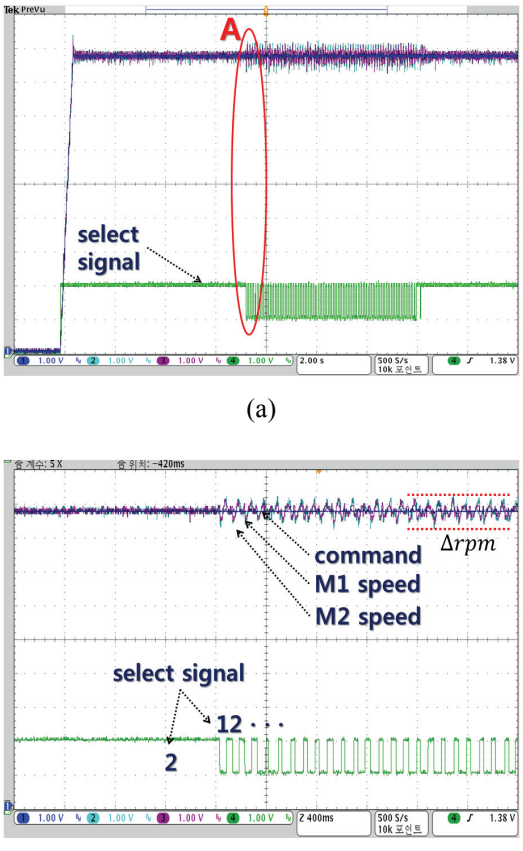

Fig. 16. Speed response for high frequency load: (a) Speed response, (b) Zoom in region A

the rated torque was inserted to M2 at 6 s and dismissed after 2 s. After 4 s, 60% of the rated torque was again set to both motors and removed after 2 s.

Fig. 17(b) is the enlarged region A of Fig. 17(a), while Fig. 17(c) is the zoomed in region B of Fig. 17(a). Fig. 17(b) shows the speed response by difference load change, and Fig. 17(c) presents the speed response in light load conditions, in which M1 is controlled.

M1 is controlled with select signal one in initial state according to Fig. 17(b). When the load torque is set to M2 at 8 s, the controller controls M2 by toggling the select signal. The speed settling time is 192 ms and the load rate is 11.8% of the steady-state speed.

In the next step, the controller controls M1, changing the select signal to one after releasing M2 load in accordance with Fig. 17(c). The speed ripple of the steady-state occurs more than in Fig. 17(b) and is 6.3% of the steady-state speed.

The simulations and experiment show that when a relatively light load motor is controlled, the occurrence torque of the motor is less than the required torque within a 35% torque angle that can maintain a synchronized state in the parallel structure. It causes pulsations between the motors while trying to maintain a harmonized state. If the pulsation frequency for maintaining the coordinated state is collaborated with the resonant frequency occurring between the two motors, then diffusion should occur.

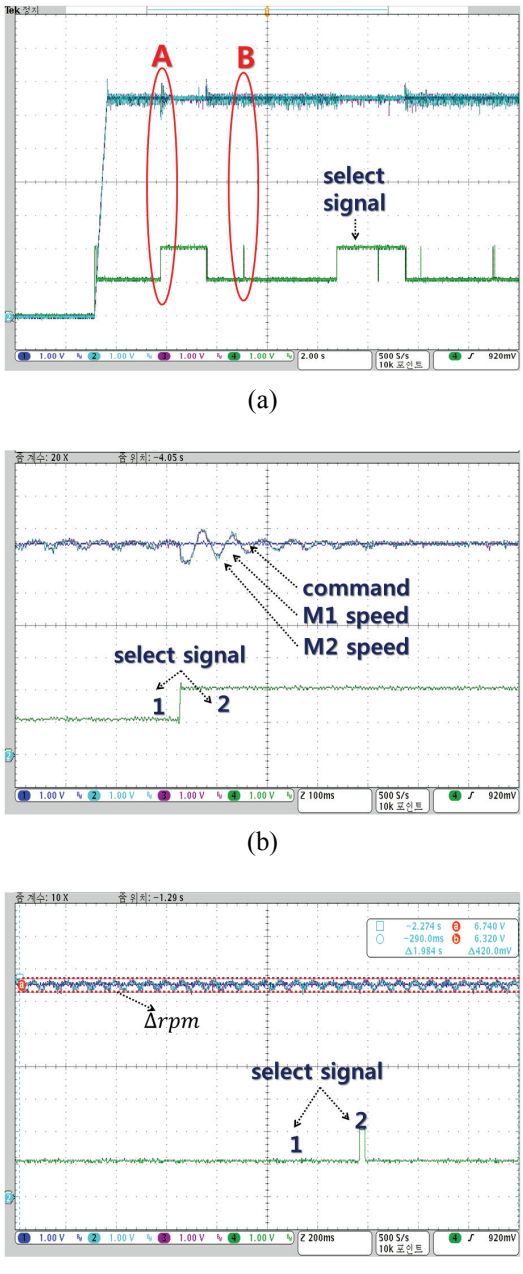

Fig. 17. Speed response for light load: Speed response; (b) Zoom in region A; (c) Zoom in region B

4. Conclusion

This paper proposed a selection control algorithm that uses flux-axis current for the stable parallel operation of SPMSMs fed by a single inverter. The proposed algorithm compares the flux-axis current of each motor, and detects the control signal from the relation between the back-EMF for torque angle and current by unbalanced load oscillation.

Unlike conventional algorithms, the proposed algorithm does not need speed sensor and hysteresis comparator, which are required in the averaged energy and rotor position error methods. The algorithm directly chooses the master motor with direct measured flux-axis current so that the dynamic characteristic in sensorless speed control is faster than that of the conventional methods.

Further, the proposed algorithm is able to stably drive the overall load torque area. It has the advantage of reduced computation because it uses only one speed controller. Finally, we verified that the proposed algorithm enables motors connected in parallel to operate stably during asynchronous load fluctuations and high frequency load change conditions via simulations with MATLAB / SIMULINK and experiment with a three-phase inverter system.

Acknowledgements

This research was supported by the Kyungpook National University Research Fund, 2012.

References

[1] E. Levi, M. Jones and S. N. Vukosavic, “Even-phase multi-motor vector controlled drive with single

inverter supply and series connection of stator windings," *IEE Pro. Electr. Power Appl.,* Vol. 150, No. 5, pp. 580-590, Sep. 2003.
[2] M. Jones, S. N. Vukosavic, D. Dujic, E. Levi, and P. Wright, "Five-leg inverter PWM technique for reduced switch count two-motor constant power applications" IET Electr. Power Appl., Vol. 2, No. 5, pp. 257-287, Sep. 2008.
[3] Hyung-Woo Lee "Study on Characteristic due to Deviation of the Wheel Diameters with Parallel Operation" *Journal of Electrical Engineering & Technology.,* Vol. 8, No. 1, pp. 106-109, Jan. 2013.
[4] A. Asri, D. Ishak, S. Iqbal, and M. Kamarol, "A speed-sensorless field oriented control of parallel-connected dual PMSM," *ICCSCE 2011. IEEE International Conference on Control System*, pp. 567-570, Nov. 2011.
[5] A. A. A. Samat, D. Ishak, P. Saedin, and S. Iqbal, "Speed-sensorless control of parallel-connected PMSM fed by a single inverter using MRAS," 2012 *IEEE International Power Engineering and Optimization Conference*, pp. 35-39, June. 2012.
[6] J. Matlagi, Z. Ibrahim, and M. Sulaiman, "Mean and differential torque control using hysteresis current controller for dual PMSM drives," *Journal of Theoretical and Applied information Technology.*, Vol. 33, No. 1, pp. 76-82, Nov. 2011.
[7] J.M. Lazi, Z. Ibrahim, M.H.N. Talib, and R. Mustafa, "Dual motor drives for PMSM using average phase current technique," *IEEE International Conference on Power and Energy (PECon2010)'2010*, pp. 786-790, Nov. 2010.
[8] D. Bidart, M. Pietrzak-David, P. Maussion, and M. Fadel, "Mono inverter dual parallel PMSM-Structure and Control strategy," *34th Annual Conference of IEEE. IECON 2008*, pp. 268-273, Nov. 2008.
[9] D. Bidart, M. Pietrzak-David, P. Maussion, and M. Fadel, "Mono inverter multi-parallel permanent magnet synchronous motor: structure and control strategy," *IET, Electric Power Applications.*, Vol. 5, No. 3, pp. 288-294, Mar. 2011.
[10] N. Matsui, T. Takeshita, and K. Yasuda, "A new sensorless drive of brushless DC motor," *in Proc. IECON '92*, pp. 430-435, 1992.
[11] N. Matsui, "Sensorless PM brushless DC motor drives," *IEEE Trans. Ind. Electron.*, Vol. 43, No. 2, pp. 300-308, Apr. 1996.
[12] Z. Chen, X. Deng, K. Huang, W. Zhen, and L. Wang, "Sensorless control of wound rotor synchronous machines based on high-frequency signal injection into the stator windings," *Journal of Power Electronics.*, Vol. 13, No. 4, pp. 669-678, Jul. 2013.
[13] A. Aimad, K. Madjid, and S. Mekhilef, "Robust sensorless sliding mode flux observer for DTC-SVM-based drive with inverter nonlinearity compensation," *Journal of Power Electronics.*, Vol. 14, No. 1, pp. 125-134, Jan. 2014.
[14] Hai Lin, Kyu-Yun Hwang, and Byung-Il Kwon, "An Improved Flux Observer for Sensorless Permanent Magnet Synchronous Motor Drives with Parameter Identification" *Journal of Electrical Engineering & Technology*, Vol. 8, No. 3 pp. 516-523, May. 2013.
[15] P. C. Sen, "Principles of electric machines and power electronics Second Edition", John Wiley & Sons, 9/ pp. 479-493, 1998

Chang-Bum Kim He received B.S degree in electrical engineering from Kyungpook National University, Daegu, Korea, in 1991, and M.S. degree in mechanical engineering, Pusan National University, Pusan, Korea, in 2003 and currently a Ph.D course student in electrical engineering with School of Electronics Engineering and work for LG electronics Inc simultaneously. His research interests are power electronics.

Chul Yun He received B.S degree in electrical engineering from Daegu University, Kyungpook, Korea, in 2010, and M.S. degree in electrical engineering with School of Electronics Engineering (SEE), Kyungpook National University (KNU), Daegu, Korea, in 2014, and currently a Ph.D course student in the same university. His research interests are motor control, power electronics.

Byung-Keun Yoon He received B.S degree in electrical engineering from Daegu University, Kyungpook, Korea, in 2010, and M.S. degree in electrical engineering with School of Electronics Engineering (SEE), Kyungpook National University (KNU), Daegu, Korea, in 2013, and currently a Ph.D course student in the same university. His research interests are motor control, power electronics.

Nae-Soo Cho He received B.S degree in electrical engineering from Kyungil university. Kyungpook, Korea, in 2001, and the M.S. and Ph.D. degree in electrical engineering with School of Electronics Engineering (SEE), Kyungpook National University (KNU). Daegu, Korea, in 2003 and 2012,

respectively. He has been with the Dept. of Electronics Information in the Keimyung College University since 2013, where he is now a Professor. His research interests are motor control and embedded systems.

Woo-Hyen Kwon He received B.S degree in electrical engineering from Sogang University. Seoul, Korea, in 1978, and the M.S. and Ph.D. degree in electrical engineering from the Korea Advanced Institute of Science and Technology(KAIST). Seoul, Korea, in 1979 and 1993, respectively. He has been with the School of Electronics Engineering (SEE), in the Kyungpook National University(KNU), since 1979, where he is now a Professor. His research interests are in the area of static power converters and drives, and computer applied systems.